Manuscript Number: AES6163

Title: Crustal thickness estimates beneath four seismic stations in Ethiopia inferred from p-wave receiver function studies

Keywords: Receiver Functions; Crustal structure; Moho; Partial melt; Anomalous Moho; Velocity model

Birhanu. A. Kibret[1] , Atalay Ayele[1] and Derek Keir[2,3]

1 Institute of Geophysics, Space Sciences and Astronomy, Addis Ababa University, Addis Ababa, Ethiopia.

2 University of Southampton, Southampton, United Kingdom.

3 University of Florence, Florence, Italy.

Abstract

Moho depths beneath four stations of the Ethiopian Seismic Station Network (ESSN) are estimated from p-wave receiver functions (RF). We used high quality seismic data recorded at ANKE (Ankober), DILA (Dilla), HARA (Harar) and SEME (Semera) stations for earthquakes located at epicentral distances ranging from 30 to 100 degrees with magnitude mb $\geq$ 5.5. We applied a frequency domain deconvolution technique to remove source and propagation path effects from the earthquakes waveforms to make the RFs dependent only on the structure beneath the seismic stations. A linearized-iterative inversion is applied on the generated radial component of the receiver functions. The minimum number of teleseismic earthquakes used is 14 for HARA while the maximum is 39 for SEME station. A linearized-iterative inversion is applied on the generated radial component of the receiver functions to obtain p-wave velocity models beneath the stations. We achieved a reasonably good fit between the observed and synthetic RFs, which demonstrated the high quality of the inversion process. From the obtained models we estimated Moho depths of 26 $\pm$ 2 km for SEME, 36 $\pm$ 2 km for DILA, 38 $\pm$ 2 km for HARA and 42 $\pm$ 1.7 km for ANKE. We have achieved a reasonably good fit between the observed and synthetic RFs which demonstrates the quality of the inversion. The lowest Moho depth is observed at Semera station which implies a thinned crust while the highest crustal thickness is observed at Ankober, which lies along the North western plateau margin. Our results agree with previous observations which strengthen the hypothesis that Moho depths estimated for stations that lie within the rift and rift margins are lower than those located in the plateaus. Our RFs inversions show a low velocity gradient at about 16km depth at Semera station, interpreted as evidence for lower crustal storage of partial melt.

1. Introduction

Most continental rifts are thought to extend by some component of mechanical extension in which faulting and stretching of the tectonic plate defines the primary architecture of the rift (Weissel and Karner, 1989). Ultimately, however, the locus of strain must shift towards a narrow zone that becomes the newly formed seafloor spreading center. It is here that magma formed from decompression melting of the mantle intrudes the plate and creates a new ocean floor (Whitehead et al., 1985). Despite the importance of continental breakup in plate tectonic theory, it remains unclear how and when the transition from mechanical to magmatic extension of the plate occur (Hayward and Ebinger, 1996; Hopper et al., 2004). For example, it is still unclear what proportion of rift extension is taken up by the intrusion and where the magma is stored in the crust beneath Afar.

In Afar, mechanical extension is thought to have initiated around ~30 Ma on large offset border faults that still define the edge of the rift (Wolfenden et al., 2004). These observations have led to the interpretation that mechanical extension by ductile stretching occurred beneath the fault bound rift (Bastow and Keir, 2011). The geological record suggests the locus of extension migrated progressively in-rift, with exposed dikes and lava flows suggesting that the progressive extension included a magmatic component. The current locus of dike intrusion (Keranen et al., 2004), recent volcanism, young faults (Corti et al., 2009), earthquakes, coupled with the geodetically constrained ground motions (Wright et al., 2006; Dumont et al., 2017) suggest extension is now mainly focused in ~20km-wide and ~50—100 km long volcanic segments that define the axis of the rift (Ebinger and Casey, 2001).

This study conducted, P to S wave conversion receiver function analysis at four newly occupied, permanent, seismic stations. Therefore, this work is aimed at estimating the Moho depth beneath Semera (Central Afar), Ankober (Northwestern plateau), Harar (Southeastern Plateau) and Dila (Southern Main Ethiopian Rift) (Figure 1) using teleseismic data recorded from September 2014 to June 2015 at Ethiopian permanent broadband seismic stations. The aims of this study is to constrain crustal thickness and internal crustal structure in the rift and adjoining plateau using passive source teleseismic receiver functions. In particular, we aim to better understand how the lower crust has been modified by magma since this has implications for the thickness, strength of extending crust, as well as for quantifying the mode of extension. Though similar receiver function studies have been done in the rift and adjoining plateaus, this work focuses on Moho depth estimation beneath three new sites with few prior constraints. We also conduct a re-appraisal of one station.

1.1 Previous constraints on crustal structure in Ethiopia

The crustal structure beneath parts of Ethiopia has been constrained using both passive and controlled source seismic techniques, such as magnetotelluric imaging, and inversion of gravity data (Didana et al., 2014; Lewi et al., 2015). Seismic imaging is in broad agreement with other geophysical methods such as magnetotelluric and gravity methods and shows that crustal thickness beneath the Northwestern plateau is 35—45km, with the thicker crustal regions along the Southern Red Sea margins and central Northwestern plateau, including up to 10km of high velocity lower crust (P-wave velocity of 7.4—7.7 km/s) (Dugda et al., 2005; Maguire et al., 2006; Stuart et al., 2006; Dugda and Nyblade, 2006; Ebinger et al., 2011). This high velocity lower crustal layer has been interpreted as "underplating" of mafic rock or high density lower crustal sill intrusion during Oligocene to Recent magmatism (Stuart et al., 2006; Cornwell et al., 2010; Maguire et al., 2006; Hammond et al., 2011; Hammond, 2014). This contrast with the South Eastern plateau where the receiver functions show the crustal thickness is consistently ~35±1 km thick (Hammond et al. 2011). From seismic refraction results Vp through the upper mantle beneath the Northwestern plateau is about 8.0 km/s (Makris and Ginzburg, 1987). We summarized previous findings of crustal thickness in Ethiopia estimated from receiver function studies in Table 1.

The crust is generally thinner and has higher Vp/Vs ratio in the Main Ethiopian Rift (MER) and Afar than the Ethiopian and Southeastern Plateau.Thickness of the crust beneath the rift reducesnorthward from ~36km in the MER, to ~25km in most of Afar, to ~15 km in northern Afar (Hammond et al., 2011). Recent multidisciplinary studies have helped to better image the crust in the region of the Tendahograben (station SEME). Magnetotelluric surveys showed the presence of a highly electrically conductive body ranging 15 to28 km depth and ~13 km width beneath the rift axis, which is in turn interpreted as evidence of considerable melt/partial melt fraction in the crust (Kind et al., 1996; Desissa et al., 2013; Didana et al., 2014; Hammond, 2014; Lewi et al., 2015). Modeling of dense micro-gravity measurements supports the presence of low density material (basaltic melt in a magma reservoir) whilst MT profile results show that high electrical conductivity material occupies space of ~13 km extent at a depth of about 15—28 km at the rift axis (Johnson, 2012. On a regional scale, the crustal thickness constrained by modeling gravity data is broadly consistent with that constrained using seismology (Tiberi et al., 2005; Mammo, 2013) (Table 2).

2. Methods

The receiver function method (RF) is a well established time series technique, which is widely used to study the structure of the Earth's crust and upper mantle (Langston, 1979; Ammon et al., 1990; Ammon, 1991). It is the transfer function between the direct P and converted S waves with all P and Ps multiples and reverberations as shown in figure (A) and (B) in Figure 3 (Ammon, 1991; Jesse and Douglas, 2004). In order to address thickness of the crust and its layered structures before and during progressive stages of rift evolution, we applied this method using high quality seismic data obtained from 4 permanent Ethiopian stations. Using Langston's [1979] source equalization procedure to remove the effects of near-source and near receiver structure are a major procedure for receiver function analysis. The procedure includes phase information, complex frequency-domain ratio and inverse transforming back into the time domain. A deconvolution approach employed in this work used a water-level stabilization method. Then, a low-pass Gaussian filter removes high-frequency noises that are not filtered by the water-level. Following a low pass Gaussian filter (reducing spectral artifacts to acquire better P-onset arrival time), rotation of the coordinates from ZNE (Z = vertical, N = north, E = east) to ZRT (Z = vertical, R = radial, T = transversal) was done to isolate the converted S phase of the direct P wave using Seismic Analysis Code (SAC) software (Goldstein, 1999). Radial and transverse receiver functions were calculated using the source equalization approach to derive the structural response beneath the recording station (Langston, 1979). This approach was done using the frequency domain water-level deconvolution method (Clayton and Wiggins, 1976; Midzi and Ottemöller, 2001).

The powerful water-level technique was done by deconvolving the vertical from radial and transverse components in the frequency domain to remove the signature of source, travel path and instrumental response effects (Langston, 1979; Ammon et al., 1990; Ammon, 1991; Dugda et al., 2005; Tuluka, 2010). Then, by multiplying the result obtained from water-level deconvolution with low-pass Gaussian filter high-frequency signals were excluded. Finally, receiver functions were stacked before being inverted to obtain the plane layered crustal velocity structure. Various starting forward velocity models ranging from 10 to 30 layers were synthetically generated for each receiver function. A smoothness factor in the range of 0.0 and 2.0 and Gaussian width factor of about 1.0 (Ammon et al., 1990; Ammon, 1991; Randall, 1989; Zandat and Ammon, 1995; Tuluka, 2010) were used to obtain a better root mean square fit between synthetic and observed receiver functions. Receiver functions were calculated using the singular-value decomposition method with a water level parameter c (in the range of 1.0 to 0.0001) to avoid division instabilities during the deconvolution process (Clayton and Wiggins, 1976; Randall, 1989; Ammon et al., 1990; Ammon, 1991; Cassidy, 1992; Mangino et al., 1993; Midzi and Ottem, 2001; Tuluka, 2010) for a better resolution of arrival times. Linearized inversion methods were used to model RF using several different starting models chosen by referring to a priori information from the previous work conducted near the study areas to make an initial model as close as the true Earth velocity structure as possible (Ammon et al., 1990). The receiver functions (RFs)) were produced using the programs written by Ammon, and others (e.g., Ammon, 1991).

By calculating the time difference between the direct P (tp) and the converted Ps (tps) phase of the receiver function plot, the crustal thickness can then be estimated by multiplying average velocity above the Moho with the time difference. This estimation provides a good "point" measurement at the station because of the steep incidence angle of the teleseismic P wave (Zhu and Kanamori, 2000).

To obtain the fittest synthetic receiver function with its corresponding inverted velocity model, we applied an iterative inversion technique that employed an initial model which presumed downward increments of velocity. We then used a gradient-based inversion algorithm to evaluate at which iteration the synthetic and observed waveforms are matched. Once we obtained the minimum number of iterations by which calculated synthetic value converges to the observed model, then that is the end of selecting a station's smoothest model that matches the observations (Ammon, 1991). The iteration halts when the calculated receiver function begins to repeat itself without having significant modification during fitting process with the observed receiver function (Ligorria and Ammon, 1999). Fittest selection criteria used in this study is by visual coherency examinations of corresponding Ps conversions of synthetic RF with stacked observed RF that is obtained by careful elimination of outliers and noisy records before the start of inversion processes (Tkalčić et al., 2011).

This work chose frequency domain over time domain method because the latter method is less efficient than simpler methods such as water level deconvolution for moderate earthquake source though it is efficient to estimate from large earthquake's source (Legorria and Ammon, 1999). The second reason we chose the frequency domain over time domain is due to the easiness of applying Water-level and Gaussian transform to limit frequency band by excluding high frequency signals (artifacts that are not obviously present in the original recording) (Langston, 1979; Clayton and Wiggins 1976) in addition to its simplicity and time efficiency (Bona, 1998). But both methods are equally effective for estimating receiver functions from high magnitude signals (Legorria and Ammon, 1999).

Frequency domain deconvolution, a spectral division technique, has an advantage to resist leakage of the low amplitude portions from P-wave receiver functions (Jeffrey and Vadim, 2000). But, it has certain shortfalls; two of these disadvantages are exposed to instability caused by the very low denominator (exposed to spectral hole) and seismic noise (Bone, 1998). To circumvent the side effect of frequency domain deconvolution, a modified spectral division is used by applying water level parameters that avoids numerical instable zeroes of the denominator (Clayton and Wiggins, 1976; Ammon, 1991; Jeffrey and Vadim, 2000). When the data are wide band with good signal to noise levels most decovolution methods such as frequency domain and time domain approaches work well, and the advantage of one method over the other is insignificant (Ligorria and Ammon, 1999) and no deconvolution approach outshines all others in all occasions and complications. In this work we used both receiver function and inverted velocity versus depth plot for a conclusion whether the point is Moho or not as Ps phase may be hidden in the noise and/or display complex masks from near-surface reverberations and P-wave multiple reflections and may not fully judged by the velocity versus plot alone (Yuan et al., 2006).

When unconsolidated sediments are unearthed below a station, the strong reverberations generated at its base mask the Ps conversions at deep structure such as the Moho. To minimize such hidden phase shift caused by masked structure we included velocity of sedimentary structure in the initial model. However, application of this technique alone didn’t fully remove the occurrences of misfit.

In this work we used both receiver functions and inverted velocity versus depth plots for a conclusion whether the point is Moho or not as Ps phase may be hidden in the noise and/or display complex masks from near-surface reverberations and P-wave multiple reflections and may not fully judged by the velocity versus plot alone (Yuan et al., 2006).

3 Results and Discussion

Using the steps and processes described in Section 2 observed waveform receiver functions were estimated for the four stations (Figure 4A). Corresponding four calculated synthetic receiver functions were chosen from the smoothest model that matches (Figure 4B) the observations by the use of visual match. From calculated smoothest models various crustal structures were obtained (Table 3).

The number of iterations in any inversion depended on the complexity of the structure and the closeness of the initial model to a structure that matches the observations (Ammon et al., 1990 and Ammon, 1991). The P wave velocity models obtained from iterative inversion technique (Figure 5) displayed the velocity contrast of ANKE, DILA, HARA and SEME stations at various depths, which describe different crustal structural units. By using good quality teleseismic signals a reliable crustal thickness and P wave velocity (Vp) contrast were estimated. However, the numerical value of Vp in SEME is not in the range of known Vp passing through Moho, the anomalous Moho depth beneath SEME station is about 26km with a Vp value of 5 km/s. This anomalous low velocity zone was obtained in the range of 15 km to 26 km deep. The station DILA located at the southern main Ethiopian rift was obtained to be the second shallowest Moho in our study with a depth of 36 km and with Vp 7.53 km/s, however, the value of Vp at different depths were found to be less heterogeneous (i.e. ranging from 6.0—7.0 km/s). There is a relatively high velocity contrast at the depth of 36km from the top beneath this station. This contrast might be due to the existence of Moho beneath DILA, a rift margin of the southeastern plateau (Mahatsente et al., 1999).

For the station HARA, which is in the southeastern plateau, there is a relatively high change in Vp from 7.8 km/s to 8.0 km/s at a depth of 38km ± 2km from the surface. The velocity contrast at this depth could be the location of the Moho interface. The Moho depth obtained in HARA is similar to the results obtained by Mahatsente et al. [1999] and Hammond et al. [2011] beneath the Southeastern plateau, which range from 36 to 38km. Significant P-wave velocity contrast of about 7.8km/s is observed at the depth of 42km ± 1.7km beneath ANKE which is thickest crust with normal Vp beneath the station and this result has a good agreement with the previous studies (Mahatsente et al., 1999; Dugda et al., 2005; Stuart et al., 2006; Hammond et al., 2011; Mammo, 2013). From inversion results of velocity versus depth a high velocity zone of about 7.1km/s is obtained in the range of ~7—10 km. The average value of Vp increases towards the Northwestern plateau and the reason for this higher than average upper crustal seismic velocity could be a mafic dike intrusion. In Figure 4B the observed and calculated receiver function obtained at HARA and SEME station look like they don't fit. This might be due to shallow volcanic and sedimentary layers which manifest high velocity contrast at its base since P wave arrivals overwhelmed by the converted phase and reverberations (Ligorria and Ammon, 1999). The locality beneath the station SEME could be layered soft and thick unconsolidated sediment that mixes the direct P and converted Ps phase (Chen and Niu, 2016).

Overall, the thinnest crust is observed in SEME with the existence of anomalous Moho, while the thickest crust is in the Northwestern plateau beneath ANKE with the observed normal Moho (Table 3). Similar patterns of Moho depths were found near these two localities in previous studies (Dugda and Nyblade, 2006; Stuart et al., 2006; Cornwell et al., 2010). From the velocity models obtained from the inversion process, the top most crustal layer of about 4 km at SEME has a very low velocity, Vp. Beneath this low velocity there is a high velocity (~6.6 km/s—7.6 km/s) thick crustal layer of about 8km thick. At 16km the velocity decreases steeply to a low velocity layer of about 10km thick. The anomalous Moho depth beneath SEME station is about 26km ± 2km, while the Moho depth beneath ANKE is at the depth of 42km ± 1.7km.

The crustal structure observed beneath SEME is distinctly different from that observed under the other three stations. The upper crustal layers in the top 4km have very low P wave velocities ranging from 2.4 to 3.2 km/s. This might be interpreted as a cover sediment (maybe evaporates) or volcanic layer. Top most layers beneath SEME are likely to be volcanic rocks intercalated with thin sediments. This is similar to the results obtained by Lewi et al. [2015] for a site with surface sediments of a thickness not more than 1.2 km is decreasing to 0.75 km northwards.

Beneath this station a high velocity layer (~7—7.6 km/s) between 6 km to 14km is consistent with the presence of cooled magmatic intrusion. Below this high velocity zone, a very low Vp value was obtained (Figure 6) in the depth range of 16 km—26 km, which is unusual compared to earlier receiver function studies near the area (Dugda et al., 2005; Dugda and Nyblade, 2006; Stuart et al., 2006; Hammond et al., 2011; Hammond, 2014). Forward modeling shows that the observed very low velocity is not an artifact of the inversion process, but can potentially be explained by deep seated fluid accumulation. This conclusion is justified by the fact SEME station is located at the southeastern terminus of the active Manda Hararo Rift system which is near the Tendaho basin where deep seated magma and hydrothermal reservoirs are potentially possible at the specified depth (Hernández-Antonio et al., 2015). A similar inference is given by Field et al. [2012] as there isperalkaline magmas beneath Dabbahu Volcano, Afar. Using secondary ion mass spectrometry (SIMS) analysis of volatile contents in melt inclusions (Kind et al., 1996) and olivine from pantellerite obsidians which represent the youngest eruptive phase (<8 ka) that includes H_2O contents ≤5.8 wt. % and CO_2 contents below 500 ppm (Field et al., 2012). Petrological methods for constraining magma storage depths include the identification of dissolved volatiles (principally H_2O and CO_2) in phenocryst-hosted melt inclusions from Dabbahu, which are H_2O-rich in the range of 3 to 5.8 wt.%. However, high magmatic H_2O is consistent with other findings in peralkaline rocks (Maksimov, 2008; Blundy and Cashman, 2008; Field et al., 2012) in Dabbahu near SEME station. Touret and Van Den Kerkhof [1986] gave a possible evidence for the presence and the nature of free fluid phase to be found at depths down to 35 km below the surface of the continent. The existence of melt and/or fluid beneath SEME makes the anomalous Moho difficult (since observed Vp value beneath SEME is very small compared to global Moho velocity) to identify only using Vp value from the velocity versus depth plot alone unless a priori Vp value is used. However, the source of this low velocity beneath the station could be the release of magmatic fluid such as CO_2 and H_2O from the mantle to the crust (Bucher-Nurminen, 1990). This inference may get accompanied by either the accumulation of H_2O-rich fluid composition, heat and/or volatile in the lower crust (Zandt and Ammon, 1995) which percolates upwards through the crust by a porous-media or fracture depending on the melting of the crust. If the temperature of the lower crust is high enough, this fluid could induce partial melting of material of suitable composition (Amundsen, 1987; Bucher-Nurminen, 1990). This has a similar inference with the work of Thompson and Connolly [1990] as fluid accumulation is a common phenomenon in the lower crust. The maximum fluid content transferred from the mantle to the lower crust depends on both Moho temperature and depth (Bucher-Nurminen, 1990). The existence of the partial melt in the lower crust beneath Afar is supported by previous geophysical studies such as Hammond et al.

[2011], Guidarelli et al. [2011], Desissa et al. [2013] and Hammond [2014], which are interpreted as stored melt in the sill-like features in the lower crust.

The Moho depth beneath SEME is about 26km ± 2km and the result is very close to an inference given by (Berckhemer, 1975). Gravity modeling in the southern central part and margin of the Red Sea Rift shows that there is a possibility of partial melt existence at a depth of 8.5 to 25 km (Johnson, 2012; Lewi et al., 2015). In their work, Knox et al. (1998) used the inversion of Rayleigh wave dispersion and found low S-wave velocities (0.2—0.8 km/s) and that were inferred as partial melt.

4 Global comparisons and the major points

Crustal P wave seismic velocities and crustal thicknesses observed beneath HARA and DILA are similar to the global average crustal structure (Christensen and Mooney, 1995), suggesting that the crust on the Southeastern side of the MER and Afar have not been significantly modified by plate thinning and intrusion. The relatively normal seismic velocities in the crust make a relatively sharp contrast with what is slower than the global average upper mantle seismic velocities.

ANKE is characterized by a 42 km thick crust that has higher seismic velocities than HARA and DILA, and thus higher than the global average. Specifically, the observed velocities at 5—10 km depth is ~0.5 to 1 km/s faster than the globally most commonly observed range of 6—6.5 km for this depth range [e.g., Christensen and Mooney, 1995]. In addition, the seismic velocities of ~7km/s in the 30-40 km deep lower crust is towards the higher end of the globally most common velocities of 6.5—7.1 km/s. Since frozen mafic rock has a seismic velocity of over 7 km/s, the modification of the crust at ANKE by mafic intrusion provides a simple explanation for high seismic velocity through lower crust underplating and recent magmatic activity beneath the Northwestern plateau (Mackenzie et al., 2005). Intruded upper crust is consistent with observed mafic dykes exposed near the surface along the western margin of Afar (Wolfenden et al., 2004). Elevated lower crustal velocities are consistent with the presence of frozen lower crustal, stacked sill complexes imaged beneath the western margin of the MER and the Northwestern plateau by controlled source and passive seismic techniques in project EAGLE (Stuart et al., 2006; Keir et al., 2009). In light of previous results, the observed crustal structure beneath ANKE is consistent with the interpretation that the crust beneath the northwestern side of Afar and the MER has been significantly modified by magmatism. Our results suggest that intrusion into the upper crust along the western Afar margin may be more significant than previously thought.

The seismic velocity structure of SEME is quite different to the other seismic stations, and to the global average continental crust. Seismic velocities in the uppermost crust are exceptionally low, consistent with the presence of a sedimentary basin including evaporites. Seismic velocities at 10—13 km depth are over 7 km/s, and consistent with the presence of upper crustal mafic intrusion. Seismic velocities are then anomalously low in the 15 - 25 depth range. In light of independent constraints of high conductivities observed in MT studies at the same depth range and interpreted as evidence for the presence of partial melt (Dessiese et al., 2013), we interpret the low seismic velocities in the lower crust beneath SEME to be caused by the presence of partial melt. The interpretation is strengthened by InSAR analysis which shows a broad zone of subsidence near SEME that has been modeled as magma withdrawal from a lower crustal sill complex (Grandin et al., 2009). Our observations, in light of previous constraints from Afar as well as from seismic refraction images across rifted continental margins such as the eastern north Atlantic (White et al., 2008), provides evidence that the lower crust is an important melt storage region during the breakup of continents.

Conclusions

By applying frequency domain deconvolution techniques followed by a linearized-iterative inversion on the radial component of receiver functions we obtained Moho depths of 26 ± 2 km for SEME, 36 ± 2 km for DILA, 38 ± 2 km for HARA and 42 ± 1.7 km for ANKE. We achieved a reasonably good fit between the observed and synthetic RFs by employing high quality seismic dataengaged in plain usage of water level and Gaussian filter methods. Though additive noises preceding direct P pulse caused uncertainty, the seemingly misfit result obtained at SEME and HARA stations could be due to local sediments overlaid on thick high velocity material in addition to the filters' pre-signal remnants and ambient seismic noises. The lowest Moho depth is estimated for SEME station, which implies a thinned crust while the highest crustal thickness is achieved for ANKE that lies along the Northwestern plateau margin. Our results agree with previous observations which intensify the hypothesis that Moho depths estimated for stations that lie within the rift and rift margins are lower than those located in the plateaus. Our RF inversions show a low velocity gradient at a depth of about 16km at SEME station, interpreted as evidence of lower crustal storage of partial melt, which might have a defined contribution for the transition from continental to incipient oceanic rifting. A relatively high velocity zone probably due to cooled magma from previous dike or sill intrusions is found at a depth of ~7 to 20 km at ANKE station. In contrast, Vp values beneath HARA are consistently high throughout the crust, and this might be interpreted as low crustal heterogeneity.

Acknowledgments

The authors would like to thank the technical staff of the Institute of Geophysics Space Science and Astronomy (IGSSA) Addis Ababa University. The Figs. 1 and 3 were done using Generic Mapping Tools (GMT) [Wessel and Smith, 1991]. We thank Charles Ammon for providing the inversion codes freely. We are grateful to the International Science Program of Uppsala University for financing the Ethiopian Seismic Station Network (ESSN). D.K. is supported by NERC grant NE/L013932/1.

References

Ammon, C.J., Randall, G.E., Zandt, G., 1990. On the nonuniqueness of receiver function inversions. Journal of Geophysical Research 95, 15303–15318.

Ammon, C. J., 1991. The isolation of receiver effects from teleseismic P waveforms. Bulletin of the Seismological Society of America 81, 2504–2510.

Amundsen, H.E.F., 1987. Evidence for liquid immiscibility in the upper mantle. Nature 327, 629-695.

Bastow, I.D. and Keir, D., 2011. The protracted development of the continent ocean transition in Afar. Nature Geoscience 4, 248-250.

Berckhemer, H., Baier, Bartlesen, B., Behle, A., Burkhardt, H., Gebrande, H., Markris, J., Menzel, H., Miller, H., and Vees, R., 1975. Deep seismic soundings in the Afar region and on the highland of Ethiopia, in Afar Depression of Ethiopia, 89 – 107, E. Schweizerbart, Stuttgart, Germany.

Blundy, J. And Cashman, K., 2008. Petrologic reconstruction of magmatic system variables and processes. Minerals, inclusions and volcanic processes. Mineralogical Society of America 3635 Concorde Pkwy STE 500, Chantilly, VA 20151-1125 USA pp 179–239.

Bone, M. D., 1998. Variance estimate in the frequency-domain deconvolution for teleseismic receiver function computation. Geophysics Journal International 134, 634-646 .

Bucher-Nurminen, K., 1990. Transfer of mantle fluids to the lower continental crust: Constraints from mantle mineralogy and Moho temperature. Chemical Geology, 83, 249-261.

Cassidy, J.F., 1992. Numerical experiments in broadband receiver function analysis. Bulletin of the Seismological Society of America 82, 1453–1474.

Chen, Y., and Niu, F., 2016. Joint inversion of receiver functions and surface waves with enhanced preconditioning on densely distributed CNDSN stations: Crustal and upper mantle structure beneath China. Journal of Geophysics Research Solid Earth 121, 743–766.

Christensen, N.I. and Mooney, W.D., 1995. Seismic velocity structure and composition of the continental crust: A global view. Journal of Geophysical Research 100, 9761-9788.

Clayton, R.W. and Wiggins, R.A., 1976. Source shape estimation and deconvolution of teleseismic body waves. Geophysical Journal of the Royal Astronomical Society 47, 151–177.

Cornwell, D. G., Magurie, P. K. H., England, R.W. and Stuart, G.W., 2010. Imaging detailed crustal structure and magmatic intrusion across the Ethiopian rift using a dense linear broadband array. Geochemistry Geophysics Geosystem 11.

Corti, G., 2009. Continental rift evolution: From rift initiation to incipient break-up in the Main Ethiopian Rift, East Africa. Earth Science Reviews 96(1), 1-53.

Desissa, M., Johnson, N. E., Whaler, K. A., Hautot, S., Fisseha, S. and Dawes, G. J. K., 2013. A mantle magma reservoir beneath an incipient midocean ridge in Afar, Ethiopia. Nature Geoscience 6, 861–865.

Didana, Y. L., Thiel, S. and Heinson, G., 2014. Magnetotelluric imaging of upper crustal partial melt at Tendaho graben in Afar, Ethiopia. Geophysics Research Letter 41, 3089–3095.

Dugda., M. T. and Nyblade, A. A., 2006. New constraints on crustal structure in eastern Afar from the analysis of receiver functions and surface wave dispersion in Djibouti. Geological Society of London 259, 239–251.

Dugda, M. T., Nyblade, A. A., Julia, J., Langston, C. A., Ammon, C. J., and Simiyu, S., 2005. Crustal structure in Ethiopia and Kenya from receiver function analysis: Implications for rift development in eastern Africa. Journal of Geophysical Research: Solid Earth, 110(1), 1-15

Dumont, S., Klinger, Y., Socquet, A., Doubre, C. and Jacques, E., 2017. Magma influence on propagation of normal faults: Evidence from cumulativeslip profiles along Dabbahu-Manda-Hararo rift segment (Afar, Ethiopia). Journal of Structural Geology 95, 48-49.

Ebinger, C.J. and Casey, M., 2001. Continental breakup in magmatic provinces: An Ethiopian example. Research Article 29 (6), 527-530.

Ebinger, C., Ayele, A. Keir, D., Rowland, J., Yirgu, G., Wright, T., Belachew, M., and Hamling, I., 2011. Length and Timescales of Rift Faulting and Magma Intrusion: The Afar Rifting Cycle from 2005 to Present. Annual Review of Earth and Planetary Sciences 38, 439–66.

Goldstein, P., 1999. SAC's user's manual. Lawrence-Livermore Laboratory, University of California.

Grandin, R., Socquet, A., Binet, R., Klinger, Y., Jacques, E., de Chabalier, J. B., King, G. C. P., Lasserre, C., Tait, S., Tapponnier, P., Delorme, A. and Pinzuti. P., 2009. September 2005 Manda Hararo-Dabbahu rifting event, Afar (Ethiopia): Constraints provided by geodetic data. Journal of Geophysical Research 114.

Guidarelli, M., Stuart, G., Hammond, J. O. S., Kendall, J. M., Ayele, A., and Belachew, M., 2011. Surface wave tomography across Afar, Ethiopia: Crustal structure at a rift triple-junction zone. Geophysical Research Letters 38.

Hammond, J. O. S., Kendall, J. M., Stuart, G. W., Keir, D., Ebinger, C. and Belachew, M., 2011. The nature of the crust beneath the Afar triple junction: Evidence from receiver functions. Geochemistry Geophysics Geosystem 12.

Hammond, J. O. S., 2014. Constraining melt geometries beneath the Afar Depression, Ethiopia from teleseismic receiver functions: The anisotropic H-j stacking technique. Geochemistry Geophysics Geosystem 15, 1316-1332.

Hayward, N. and Ebinger, C., 1996. Rift kinematics and along-axis segmentation in northern Afar. Tectonics, 15, 244-257.

Hernández-Antonio, A., Mahlknecht, J., Tamez-Meléndez, C., Ramos-Leal, J., Ramírez-Orozco, A., Parra, R., Ornelas-Soto, N., and Eastoe, C. J., 2015. Groundwater flow processes and mixing in active volcanic systems: the case of Guadalajara (Mexico). Hydrology and Earth System Science 19, 3937-3950.

Hopper, J.R., Funck, T., Tucholke, B.E., Larsen, H., Holbrook, W.S., Louden, K.E., Shillington, D. and Lau, H., 2004. Continental breakup and the onset of ultra slow seafloor spreading off Flemish Cap on the Newfoundland rifted margin. Geology 32 (1), 93–96.

Jeffrey, P. and Vadim, L., 2000. Receiver Functions from Multiple-Taper Spectral Correlation Estimates. Bulletin of the Seismological Society of America 90(6), 1507–1520.

Jesse, F. L. and Douglas A.W., 2004. Combined Receiver-Function and Surface Wave Phase-Velocity Inversion Using a Niching Genetic Algorithm: Application to Patagonia. Bulletin of the Seismological Society of America 94, 977–987.

Johnson, N., 2012. Magnetotelluric studies of the crust and upper mantle in a zone of active continental breakup, Afar, Ethiopia. PhD thesis, University of Edinburgh.

Keir, D., Hamling, I., Ayele, A., Calais, E., Ebinger, C., Wright, T.J., Jacques, E., Mohammed, K., Hammond, J.O.S., Belachew, M., Baker, E., Rowland, J.V., Lewi, E. And Bennati, L., 2009. Evidence for focused magmatic accretion at segment centers from lateral dike Injections captured beneath the Red Sea rift in Afar. Geology 37, 59–62.

Keranen, K., Klemperer, S.L., Gloaguen, R., Asfaw, A., Ayele, A., Ebinger, C., Furman,T., Harder, S., Keller, G.R., Mackenzie, G.D., Maguire, P.K.H., and Stuart, G.W., 2004. Three-dimensional seismic imaging of a protoridge axis in the Main Ethiopian rift. Geological Society of America 32, 949–952.

Kind, R., Ni, J., Zhao, W., Wu, J., Yuan, X., Zhao, L., Sandvol, E., Reese, C., Nabelek, J. and Hearn, T., 1996. Evidence from earthquake data for a partially molten crustal layer in southern Tibet. Science 274(5293), 1692–1694.

Knox, R., Nyblade, A. and Langston, C., 1998. Upper mantle S velocities beneath Afar and western Saudi Arabia from Rayleigh wave dispersion. Geophysical Research Letters 25, 4233–4236.

Langston, C. A., 1979. Structure under Mount Rainier, Washington, inferred from teleseismic body waves. Journal of Geophysical Research 84, 4749–4762.

Legorria, J. P. and Ammon, C. J., 1999. Iterative Deconvolution and Receiver-Function Estimation. Bulletin of the22 Seismological Society of America 89(5), 1395- 1400.

Lewi, E., Keir, D., Birhanu, Y., Blundy, J., Stuart, G., Wright, T., and Calais, E., 2015. Use of a high-precision gravity survey to understand the formation of oceanic crust and the role of melt at the southern Red Sea rift in Afar, Ethiopia. Geological Society of London 20.

Mackenzie, G.H., Thybo, G.H. & Maguire, P., 2005. Crustal velocity structure across the Main Ethiopian Rift: results from 2-dimensional wide-angle seismic modeling, Geophysical Journal International 162, 994-1006.

Maguire, P.K.H., Keller, G.R., Klemperer, S.L.,Mackenzie, G.D., Keranen, K., Harder, S.,O'Reilly, B., Thybo, H., Asfaw, L., Khan, M.A., and Amha, M., 2006. Crustal structure of the northern Main Ethiopian Rift from the EAGLE controlled source survey; a snapshot of incipient lithospheric break-up. Geological Society of London 259, 269–291.

Mahatsente, R., Jentzsch, G. and Jahr, T., 1999. Crustal structure of the Main Ethiopian Rift from gravity data: 3-dimensional modeling. Tectonophysics 313, 363–382.

Makris, J. and Ginzburg, A., 1987. The Afar Depression: Transition between continental rifting and seafloor spreading. Tectonophysics 141, 199–214.

Maksimov, A. P., 2008. A Physicochemical Model for Deep Degassing of Water-Rich Magma, Journal of Volcanology and Seismology 2, 60 - 68.

Mammo, T., 2013. Crustal Structure of the Flood Basalt Province of Ethiopia from Constrained 3-D Gravity Inversion. Pure and Applied Geophysics 1–22.

Mangino, S. G., Zandt, G. and Ammon, C. J., 1993. The receiver structure beneath Mina,Nevada. Bulletin of the Seismological Society of America 83, 542–560.

Midzi, V. and OttemöoEller, L., 2001. Receiver function structure beneath three southern Africa seismic broadband stations. Tectonophysics. 339, 443–454.

Randall, G. E., 1989. Efficient calculation of differential seismograms for lithospheric receiver functions. Geophysics Journal International 99, 469–481.

Stuart, G., Bastow, I. D. and Ebinger, C. J., 2006, Crustal structure of the northern Main Ethiopian Rift from receiver function studies, in The Afar Volcanic Province Within the East African Rift System, edited by G. Yirgu, C. J. Ebinger, and P. K. H. Maguire. Geological Society Special Publications 259, 253–267.

Thompson, A. B. and Connolly, J. A. D., 1990. Metamorphic fluids and anomalous porosities in the lower crust. Tectonophysics, 182, 47 - 55.

Tiberi, C., Ebinger, C., Ballu, V., Stuart, G., and Oluma, B., 2005. Inverse models of gravity Data from the Red Sea-Aden-East African rifts triple junction zone, Geophysical Journal International, 163 , 775–787.

Tkalčić, H., Chen, Y., Liu, R., Zhibin, H., Sun, L. and Chan, W., (2011). Multistep modelling of teleseismic receiver functions combined with constraints from seismic tomography: crustal structure beneath southeast China. Geophysics Journal International 187, 303–326.

Touret, J. And Van Den Kerkhof, A. M., 1986. High Density Fluids in the Lower crust and Upper mantle. Physica 139 and 140B, 834-840.

Tuluka, J. M., 2010. Crustal structure beneath two seismic broadband stations revealed from teleseismic P-wave receiver function analysis in the Virunga volcanic area, Western Rift Valley of Africa. Journal of African Earth Sciences 58(5), 820-828.

Weissel, J. K. and Karner G. D., 1989. Flexural uplift of rift flanks due to mechanical unloading of the lithosphere during extension. Journal of Geophysical Research 94, 919-950.

Wessel, P. and Smith, W. H. F., 1991. Free software helps map and display data. EOS Trans. American Geophysical Union 72(41), 441.

White, R. S., Smith, L. K., Roberts, A. W., Christie, P. A. F., Kusznir, N. J. and the rest of the iSIMM Team., 2008. Lower-crustal intrusion on the North Atlantic continental margin. Nature 452(27), 460-465.

Whitehead, J.A., Dick, H.J.B., and Scouten, H., 1985. A mechanism for magmatic accretion under spreading centers. Nature 312, 146–148.

Wolfenden, E., Ebinger, C., Yirgu, G., Deino, A., and Ayalew, D., 2004. Evolution of the northern Main Ethiopian Rift: Birth of a triple junction. Earth and Planetary Science Letter 224, 213–228.

Wright, T. J., Ebinger, C., Biggs, J., Ayele, A., Yirgu, G., Keir, D., 2006. A Stork Magma maintained rift segmentation at continental rupture in the 2005 Afar dyking episode. Nature 42, 291-294.

Yuan, X., Kind, R., Li, X., Wang, R., 2006. The S receiver functions: synthetics and data example. Geophysical Journal International 165, 555–564.

Zandt, G. and Ammon, C. J., 1995. Continental Crustal composition constrained by measurements of crustal Poisson's ratio. Nature 374, 152–154.

Zhu, L. and Kanamori, H., 2000. Moho Depth Variation in Southern California from Teleseismic Receiver Functions. Journal of Geophysical Research 105, 2969–2980.

Figures

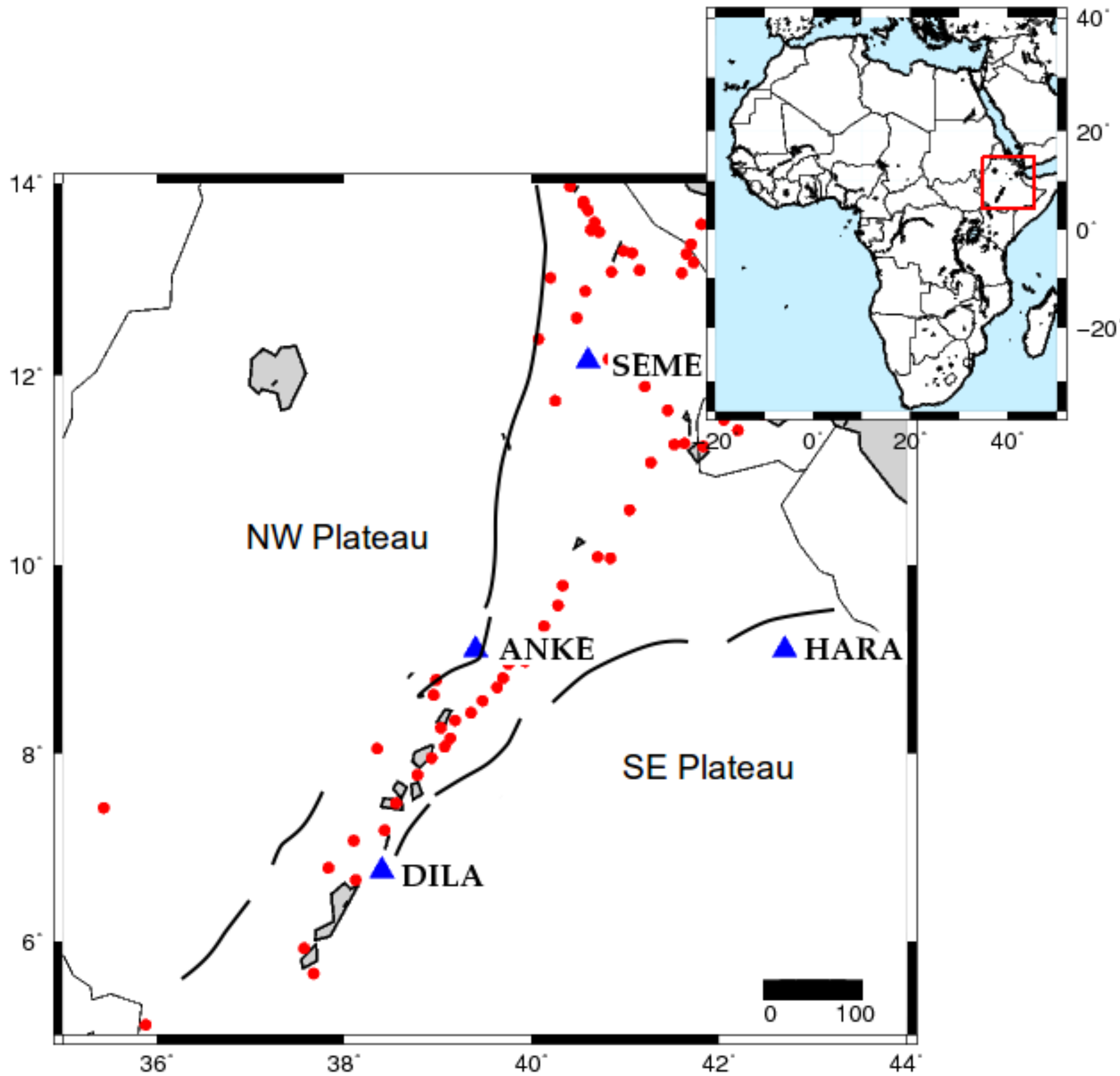

Figure 1. Location of the four Ethiopian permanent broadband seismic stations (blue triangles) for which receiver functions and P wave velocity models were estimated. The black thick lines are border faults that separate the NW plateau and the SE plateau from the Main Ethiopian Rift and Afar. The red circles represent the location of volcanoes. Inset: The red rectangle shows the location of the study area on the African continent

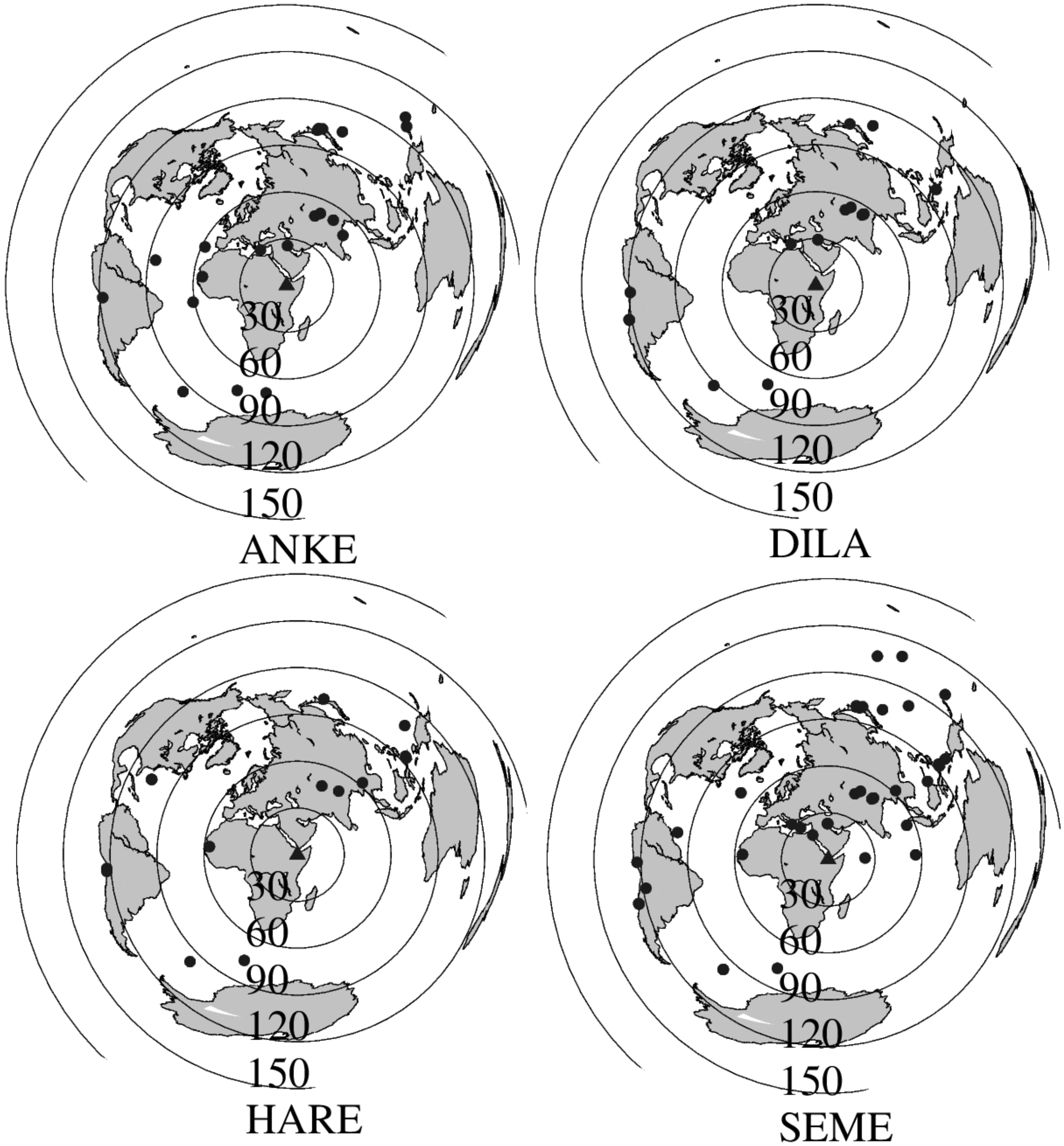

Figure 2. The solid black circular symbols are the locations of the teleseismic earthquakes that occurred between September 2014 and August 2015 with a magnitude greater than or equal to 5.5mb and within epicentral distances between 30ºand 100º. These earthquake data were recorded by the Ethiopian permanent broad band seismic network of stations (ANKE, SEME, HARA and DILA) and collected by the team led by the Institute of Geophysics Space Science and Astronomy (IGSSA), Addis Ababa University. The black triangles in the center of the internal circles are locations of each seismic station. The teleseismic earthquake's information (latitude, longitude and magnitudes) were taken from Global Earthquake catalog of the International Earthquake Information Center.

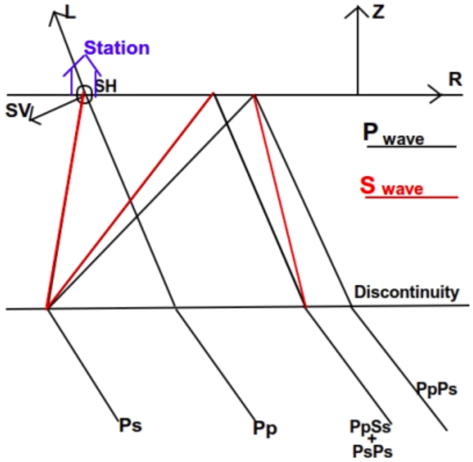

(A)

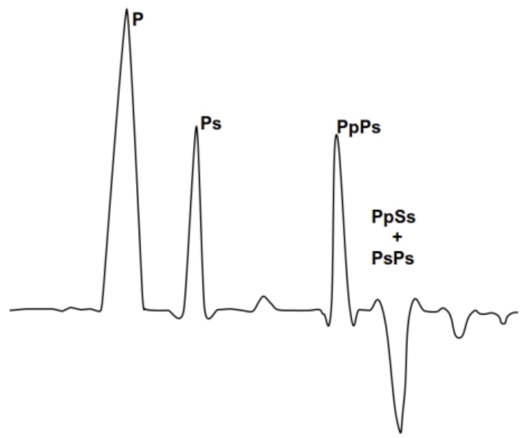

(B)

Figure 3. (A) is a graphical representation ray diagram of receiver functions identifying the major P- to S converted phases that illustrates the direct P, Ps, PpPs and PpSs phases that comprises the receiver function for a single half-space and (B) is a receiver function that shows the direct P-wave and the reverberations (Ps, PpPs, PsPs + PpSs).

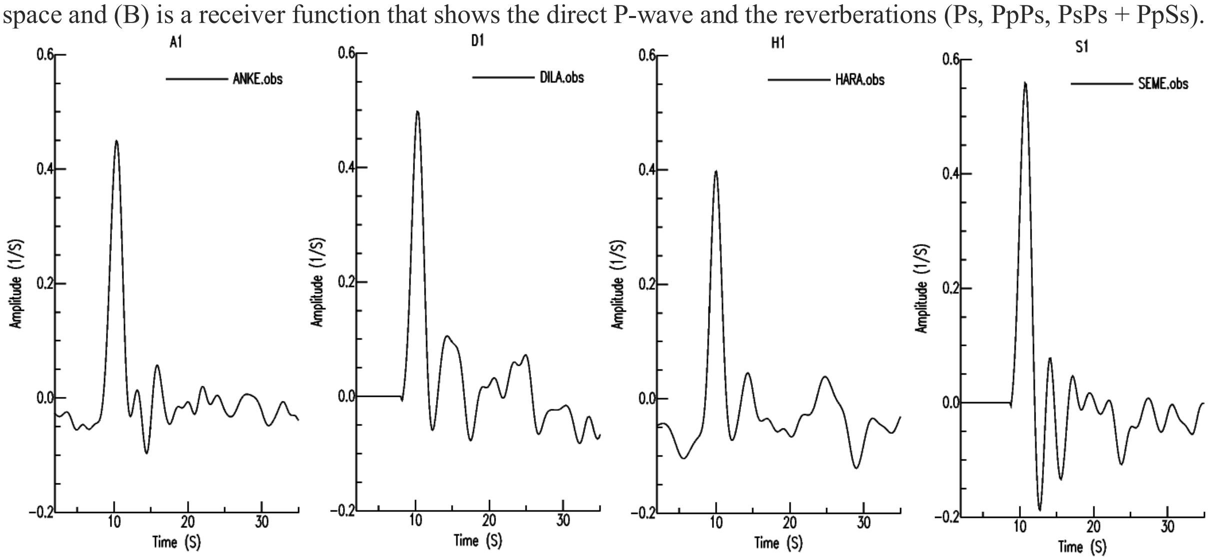

(A)

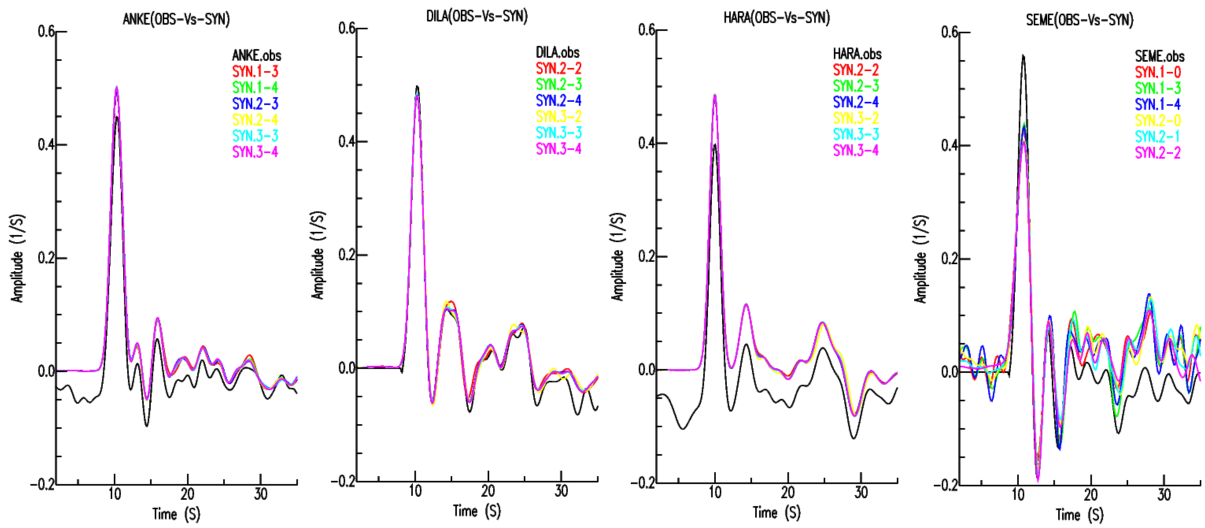

(B)

Figure 4. (A)The black wave form represented by A1, D1, H1 and S1 are the observed waveform receiver functions obtained from the deconvolution of the radial component from the horizontal component waveform of the teleseismic earthquakes recorded at ANKE, DILA, HARA and SEME permanent broad band seismic stations. (B) Observed receiver functions (Figure A) fit with the synthetic coloured receiver functions obtained from iterative frequency domain water level deconvolution technique. In all plots the delay time given for the P wave to show contrast is 10 seconds and Ps marked in each plot is the conversion from direct P wave to S wave. The coloured waveform models are the synthetic receiver functions obtained by varying the smoothing weight parameters using the program "smthinv".

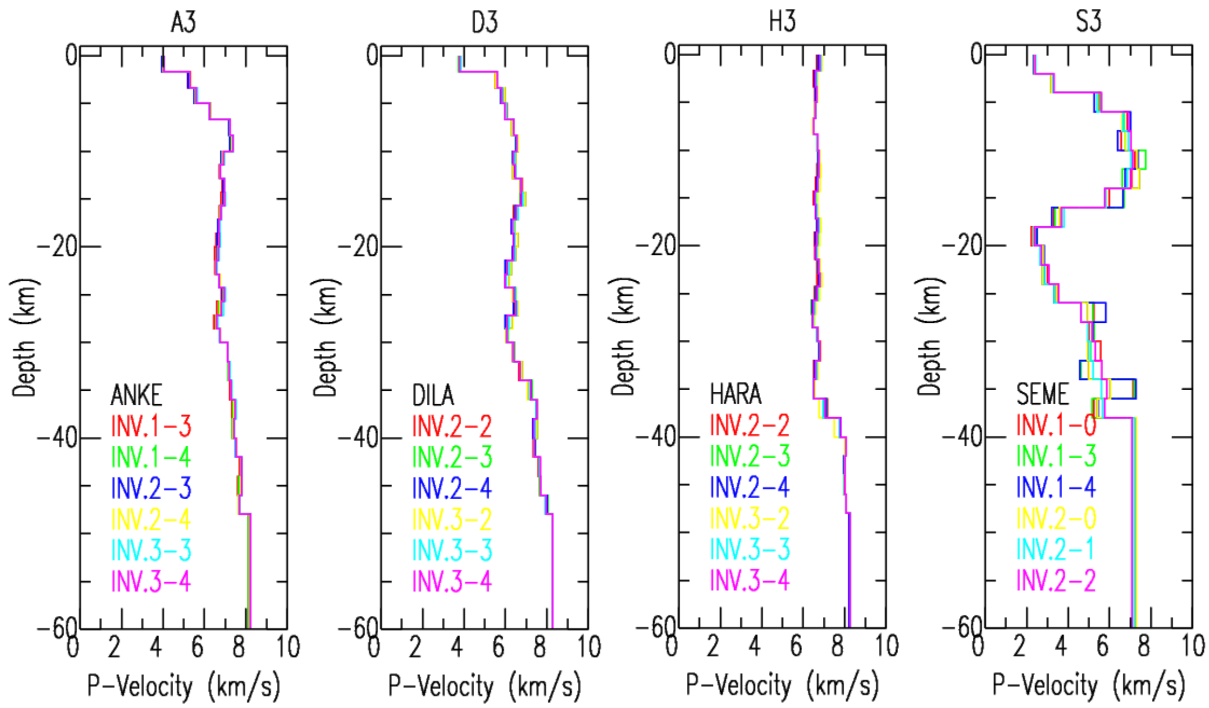

Figure 5. P wave velocity models obtained by inverting receiver functions for the seismic stations A3 (ANKE), D3 (DILA), H3 (HARA) and S3 (SEME). The inversion results in these plots were obtained using programs by Ammon[1991]. The Moho is interpreted as the depth at which there is a sharp increase in seismic velocity from ~6.5 km/s in the lower crust to 7—7.5 km/s in the upper mantle.